may have created one more, particularly the π type. Hence, the band at 22 990 cm^{-1} has been assigned to $L_\pi \rightarrow M$.

The band at 26 570 cm^{-1} is the only forbidden charge-transfer transition from ligand to metal that we could observe in $[Ni(mnt)_2]^{2-}$. The difficulty in the assignment of this band by the earlier workers could have come from the fact that this band in combination with an allowed band at 27 060 cm^{-1} forms a very broad absorption with a full width at half-maximum of nearly 7000 cm^{-1}, making it difficult to even guess the presence of two components. However, our polarized optical work in combination with the low-temperature work clearly brings out the forbidden nature of the former band and the allowedness of the latter. Particularly the temperature-dependence study indicates the combination of the 26 570- and 27 060-cm^{-1} bands at room temperature, which progressively shows the evolution of the 27 060-cm^{-1} band accompanied by the disappearance of the 26 570-cm^{-1} band (Figure 4a). This must have caused Shupack et al.[12] to assign the broad band as their transition $L_\pi \rightarrow M$ ($2b_{3u}$, $2b_{2u} \rightarrow 3b_{1g}$). Though this assignment is wrong for the parallel-polarized band at 26 570 cm^{-1}, it holds good for the perpendicularly polarized one at 27 060 cm^{-1}. Similarly, Schrauzer and Mayweg assigned a band similar to 26 570 cm^{-1} in $[Ni(mnt)_2]^-$ to $^1A_g \rightarrow {}^1B_{1g}$ ($n_{=S} \rightarrow M$). We concur with their assignment for the forbidden band at 26 570 cm^{-1}. Moreover, some of the charge-transfer transitions in the square-planar halide complexes are known to be of $L \rightarrow M$ type.[36] Typically they exhibit two bands separated approximately by 10 000 cm^{-1} with higher energy bands being considerably more intense. Our assignment of this band at 27 060 cm^{-1} is in complete accord with that of Shupack et al.[12] as an $L \rightarrow M$ charge-transfer transition, while the other transition of the same type does occur at high energy, 38 600 cm^{-1}. The band at 31 850 cm^{-1} is an $L \rightarrow L^*$ transition since it corresponds to the first absorption in bis((methylthio)maleonitrile) at about 30 000 cm^{-1}.[12]

C. Temperature Dependence from 18 to 50 K. It is quite surprising that the intensities of all the transitions increase below 50 K. This could be tentatively interpreted as due to a lowering of the symmetry of the complex ion, making all the transitions allowed. The following experimental facts lend support to this tentative conclusion: (i) no new transitions have been observed at temperatures below 50 K; (ii) the bands observed above 50 K do not disappear when the system is cooled below 50 K; (iii) some of the bands moved to lower energies at temperatures below 50 K. The increase in intensity accompanied by a decrease in transition energies can hence be explained by a departure from the planarity of $Ni(mnt)_2^{2-}$ anion. In other words, the symmetry of the anion responsible for the entire electronic spectrum could have changed from D_{2h} to D_2 by creating a dihedral angle between the two ligand planes attached to the same metal atom. Such exceptional nonplanarity has been found in some of the dithiolene complexes.[38-42]

Recently we have observed two phase transitions,[43] one at 50 K and another around 20 K, when we studied the ESR of $Cu(mnt)_2^{2-}$ doped in $[(n\text{-}Bu)_4N]_2[Ni(mnt)_2]$. The carefully measured ESR spectra further reveal a slight change in the "g" and "A" tensors of the $Cu(mnt)_2^{2-}$ ion, giving evidence to distortions from planarity. Detailed work is under way.

Conclusions

A combination of the polarized spectra of single crystals of $[(n\text{-}Bu)_4N]_2[Ni(mnt)_2]$ with a low-temperature isotropic study has thrown considerable light on the rich electronic spectra of the complex ion. Though we have interpreted the electronic spectra on the basis of a scheme proposed by us, the rich optical spectral data necessitates a new molecular orbital calculation in order to confirm the nature of electronic excitations suggested in this work. Furthermore, experiments below 50 K suggest the deviation of this dithiolene complex from planarity.

Acknowledgment. We gratefully acknowledge the Department of Science and Technology, Government of India, for financial support to carry out this work.

Registry No. $[(n\text{-}Bu)_4N][Ni(mnt)_2]$, 18958-57-1.

(38) Snaathorst, D.; Doesburg, H. M.; Perenboom, J. A. A. J.; Keijzers, C. P. *Inorg. Chem.* **1981**, *20*, 2526.
(39) Venkatalakshmi, N.; Babu Varghese; Williams, R. F. X.; Manoharan, P. T., unpublished observations.
(40) Hamilton, W. C.; Bernal, I. *Inorg. Chem.* **1967**, *6*, 2003.
(41) Enemark, J. H.; Lipscomb, W. N. *Inorg. Chem.* **1965**, *4*, 1729.
(42) Baker-Hawkes, M. J.; Dosi, Z.; Eisenberg, R.; Gray, H. B. *J. Am. Chem. Soc.* **1968**, *90*, 4253.
(43) Chandramouli, G. V. R.; Manoharan, P. T., unpublished results.

Contribution from the Department of Chemistry, Colorado State University, Fort Collins, Colorado 80523

Theoretical Characterization of Nitrogen Fixation: Effect of Ligand on the Initial Dinitrogen Activation

A. K. Rappé

Received May 9, 1986

Correlated ab initio theoretical calculations at the valence double-ζ level are used to study the effect of metal (molybdenum and tungsten) and ligand (fluorine, chlorine, and bromine) on the relative stability of activated (azine) vs. unactivated forms of bridging dinitrogen. We find a pronounced (26 kcal/mol) effect of halogen substitution for the molybdenum complexes $[MoX_4N]_2$. For the tungsten analogues we find only a minor variation (9 kcal/mol) with halogen substitution. For all three halogen complexes the activated form of N_2 (azine) is substantially more stable than the unactivated classical structure for tungsten. For molybdenum, even with halogen variation the unactivated form is more stable than the activated form.

Introduction

The activation and reduction of dinitrogen under mild conditions is a process of interest in heterogeneous catalysis,[1] homogeneous reactivity and structural studies,[2-10] and theoretical studies.[11-17]

$$N_2(g) + 3H_2(g) \rightarrow 2NH_3(g) \quad (1)$$

The ΔG_{300K} for this reaction is -7.9 kcal/mol.[18] Industrially, this

(1) (a) Ertl, G. *Catal. Rev.—Sci. Eng.* **1980**, *21*, 201-223. (b) Boudart, M. *Catal. Rev.—Sci. Eng.* **1981**, *23*, 1-15. (c) Nieken, A. *Catal. Rev.—Sci. Eng.* 17-51. (d) Ozaki, A. *Acc. Chem. Res.* **1981**, *14*, 16-21. (e) *Riegel's Handbook of Industrial Chemistry*; Kent, J. A., Ed.; Van Nostrand Reinhold: New York, 1983; pp 143-221.

(2) (a) Chatt, J.; Dilworth, J. R.; Richards, R. L. *Chem. Rev.* **1978**, *78*, 589-625. (b) Henderson, R. A.; Leigh, G. J.; Picket, C. J. *Adv. Inorg. Chem. Radiochem.* **1983**, *27*, 197-292.

0020-1669/86/1325-4686$01.50/0

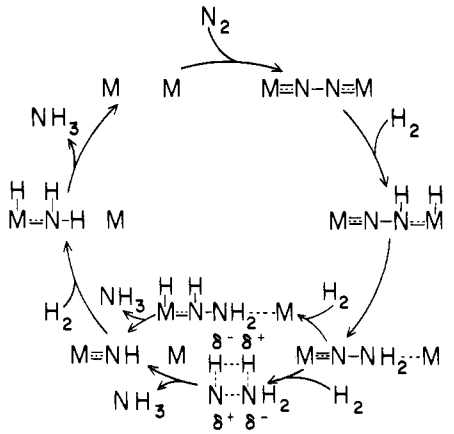

Figure 1. Suggested ammonia synthesis scheme.

reaction is run at high temperatures (400–800 °C) and pressures (100–1000 atm) with the aid of a heterogeneous iron catalyst.[1] High pressures are required to operationally offset the unfavorable equilibrium imposed by the high temperatures needed to kinetically facilitate the reaction (E_a ranges from 17 to 29 kcal/mol[1]); at 1 atm pressure $\Delta G_{800K} = +18.5$ kcal/mol, and at 200 atm pressure $\Delta G_{800K} = +1.7$ kcal/mol. The high pressure associated with current industrial dinitrogen reduction represents a major source of energy expenditure. A long-term solution to these energy requirements is to design a catalytic system that will reduce (hydrogenate) dinitrogen under ambient conditions. The smaller activation energy would then permit lower temperatures, which would in turn permit lower pressures.

Much of the homogeneous experimental[2,4] and theoretical work[11-13,15] has been concerned with structural and reactivity studies of terminal and bridging dinitrogen ligands having intact N–N π bonds. Experimentally, strong acids are required for reaction with the intact N–N π bond. Although these studies may have relevance as functional and/or structural models of nitrogenase,[2] they are not likely to lead to solutions to the energy-intensive industrial nitrogen fixation problem. Other experimental[5-10] and theoretical[14] work has been concerned with understanding highly unsymmetrical bridging environments; again, reaction with strong acid is required for reduction of the dinitrogen ligand, though for these systems the N–N bond is substantially lengthened. There is a very recent report wherein Hoffmann and co-workers[16] observe an activated form of N_2 using extended Hückel theory, in agreement with our previous work.[17]

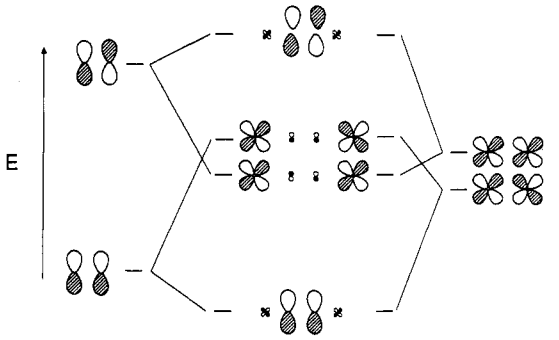

Figure 2. Orbital correlation diagram for combining the π orbitals of dinitrogen with the π orbitals of a metal dimer to form a classical bridging dinitrogen complex.

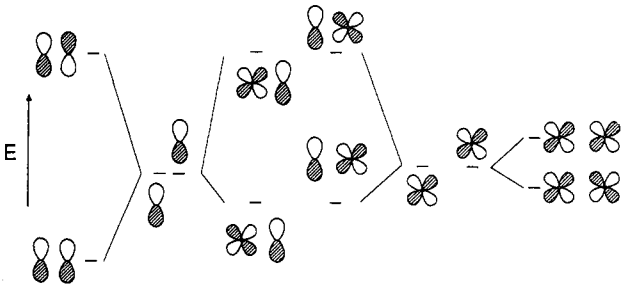

Figure 3. Orbital correlation diagram for combining the π orbitals of dinitrogen with the π orbitals of a metal dimer to form an activated (azine) form of bridging dinitrogen complex. The nitrogen and metal π and π^* orbitals are precombined to form localized orbitals that are appropriate for forming localized M–N π bonds.

We have studied[17] reaction schemes that are predicted to be reactive enough for dihydrogen to be at least a potential reductant. One such scheme is outlined in Figure 1 and is based on the discovery by Schrock and co-workers[3] of a symmetrically activated form of dinitrogen containing the valence-bond structural unit

$$M{\equiv}N{-}N{\equiv}M$$

1

Because metal–ligand π bonds, in general, are vastly more reactive than analogous fully organic π bonds,[19] we expect **1** to be more reactive than the classical structure[2] with an intact N–N π bond

$$M{-}N{\equiv}N{-}M$$

2

Formation of the activated structure **1** will require considerable electronic reorganization and will be found only with ligands that stabilize metal–ligand π bonding. The electronic structure of **1** is reasonably well described by a modification of the correlation diagram in Figure 2 wherein the nitrogen π and π^* orbitals and metal π and π^* orbitals are recombined before the fragments are mixed to form the molecule; this is shown in Figure 3. In the

(3) (a) Turner, H. W.; Fellman, J. D.; Rocklage, S. M.; Schrock, R. R.; Churchill, M. R.; Wasserman, H. J. *J. Am. Chem. Soc.* **1980**, *102*, 7809–7811. (b) Churchill, M. R.; Wasserman, H. J. *Inorg. Chem.* **1981**, *20*, 2899–2904. (c) Churchill, M. R.; Wasserman *Inorg. Chem.* **1982**, *21*, 218–222. (d) Rocklage, S. M.; Turner, H. W.; Fellman, J. D.; Schrock, R. R. *Organometallics* **1982**, *1*, 703–707. (e) Churchill, M. R.; Li, Y.-J.; Blum, L.; Schrock, R. R. *Organometallics* **1984**, *3*, 109–113. (f) Blum, L.; Williams, I. D.; Schrock, R. R. *J. Am. Chem. Soc.* **1984**, *106*, 8316–8317. (g) Churchill, M. R.; Li, Y.-J.; Theopold, K. H.; Schrock, R. R. *Inorg. Chem.* **1984**, *23*, 4472–4476. (h) Murray, R. C.; Schrock, R. R. *J. Am. Chem. Soc.* **1985**, *107*, 4557–4558.

(4) George, T. A.; Tisdale, R. C. *J. Am. Chem. Soc.* **1985**, *107*, 5157–5159. George, T. A.; Howell, D. B. *Inorg. Chem.* **1984**, *23*, 1502–1503. Bossard, G. E.; George, T. A.; Howell, D. B.; Koczon, L. M.; Lester, R. K. *Inorg. Chem.* **1983**, *22*, 1968–1970.

(5) Liebelt, W.; Dehnicke, K. Z. *Naturforsch., B: Anorg. Chem., Org. Chem.* **1979**, *34B*, 7–9.

(6) Cradwock, P. D.; Chatt, J.; Crabtree, R. H.; Richards, R. L. *J. Chem. Soc., Chem. Commun.* **1975**, 351–352.

(7) Pez, G. P.; Apgar, P.; Crissey, R. K. *J. Am. Chem. Soc.* **1982** *104*, 482–490.

(8) Anderson, S. N.; Richards, R. L.; Hughes, D. L. *J. Chem. Soc., Chem. Commun.* **1982**, 1291–1292.

(9) Klein, H. F.; Ellrich, K.; Ackermann, K. *J. Chem. Soc., Chem. Commun.* **1983**, 888–889.

(10) Yamamoto, A.; Miura, Y.; Ito, T.; Chen, H.-L.; Iri, K.; Ozawa, F.; Miki, K.; Sei, T.; Tanaka, N.; Kasai, N. *Organometallics* **1983**, *2*, 1429–1436.

(11) Hoffmann, R.; Thorn, D. L.; Shilov, A. E. *Koord. Khim.* **1977**, *3*, 1260–1264.

(12) Kostic, N. M.; Fenske, R. F. *J. Organomet. Chem.* **1982**, *233*, 337–351.

(13) Pelikan, P.; Boca, R. *Coord. Chem. Rev.* **1984**, *55*, 55–112.

(14) Powell, C. B.; Hall, M. B. *Inorg. Chem.* **1984**, *23*, 4619–4627.

(15) Sakaki, S.; Morokuma, K.; Ohkubo, K. *J. Am. Chem. Soc.* **1985**, *107*, 2686–2693.

(16) Wheeler, R. A.; Whangbo, M.-H.; Hughbanks, T.; Hoffmann, R.; Burdett, J. K.; Albright, T. A. *J. Am. Chem. Soc.* **1986**, *108*, 2222–2236.

(17) Rappé, A. K. *Inorg. Chem.* **1984**, *23*, 995–996.

(18) *Natl. Stand. Ref. Data Ser. (U.S., Natl. Bur. Stand.)* **1971**, *NSRDS-NBS 37*.

(19) Steigerwald, M. L.; Goddard, W. A., III *J. Am. Chem. Soc.* **1984**, *106*, 308–311. Upton, T. H. *J. Am. Chem. Soc.* **1984**, *106*, 1561–1571. Rappé, A. K.; Upton, T. H. *Organometallics* **1984**, *3*, 1440–1442. Upton, T. H.; Rappé, A. K. *J. Am. Chem. Soc.* **1985**, *107*, 1206–1218.

Table I. $[X_4MN-]_2$ Combinations of Fragment π Orbitals

X	M	structure	orbital	Nπ	Nπ*	N(π)*	N(π*)*	Mπ	Mπ*	M(π)*	M(π*)*
Cl	Mo	1	$(M-N)_1$	0.62	0.37	0.00	0.05	0.25	0.50	0.00	0.02
			$(M-N)_2$	−0.62	0.37	0.00	0.05	−0.25	0.50	0.00	0.02
			$(M-N)_1$*	0.36	0.58	0.12	0.00	−0.64	−0.49	−0.02	−0.02
			$(M-N)_2$*	−0.36	0.58	−0.12	0.00	0.64	−0.49	0.02	−0.02
Cl	Mo	2	N–N	1.00	0.00	0.02	0.00	0.00	0.00	0.00	0.00
			(M–M)*	0.00	0.07	0.00	0.01	0.00	0.99	0.00	0.01
			M–M	−0.22	0.00	−0.07	0.00	0.94	0.00	−0.01	0.00
			(N–N)*	0.00	1.00	0.00	−0.01	0.00	−0.15	0.00	−0.01
Cl	W	1	$(M-N)_1$	0.64	0.41	−0.01	0.08	0.23	0.46	0.00	0.00
			$(M-N)_2$	−0.64	0.41	0.01	0.08	−0.23	0.46	0.00	0.00
			$(M-N)_1$*	0.35	0.56	0.16	−0.04	−0.63	−0.50	0.03	0.02
			$(M-N)_2$*	−0.35	0.56	−0.16	−0.04	0.63	−0.50	−0.03	0.02
Cl	W	2	N–N	1.00	0.00	0.02	0.00	0.01	0.00	0.01	0.00
			(M–M)*	0.00	0.13	0.00	0.04	0.00	0.97	0.00	−0.01
			M–M	−0.10	0.00	0.00	0.00	1.00	0.00	0.00	0.00
			(N–N)*	0.00	1.00	0.00	−0.02	0.00	−0.21	0.00	0.03
F	Mo	1	$(M-N)_1$	0.62	0.38	0.00	0.05	0.28	0.51	0.00	0.01
			$(M-N)_2$	−0.62	0.38	0.00	0.05	−0.28	0.51	0.00	0.01
			$(M-N)_1$*	0.39	0.58	0.10	0.01	−0.64	−0.49	−0.02	−0.02
			$(M-N)_2$*	−0.39	0.58	−0.10	0.01	0.64	−0.49	0.02	−0.02
Br	Mo	1	$(M-N)_1$	0.62	0.37	0.00	0.05	0.25	0.51	0.00	−0.01
			$(M-N)_2$	−0.62	0.37	0.00	0.05	−0.25	0.51	0.00	−0.01
			$(M-N)_1$*	0.36	0.59	0.12	0.00	−0.64	−0.48	−0.02	0.01
			$(M-N)_2$*	−0.36	0.59	−0.12	0.00	0.64	−0.48	0.02	0.01
F	W	1	$(M-N)_1$	0.64	0.42	−0.01	0.08	0.24	0.46	0.00	−0.01
			$(M-N)_2$	−0.64	0.42	0.01	0.08	−0.24	0.46	0.00	−0.01
			$(M-N)_1$*	0.36	0.58	0.12	0.00	−0.63	−0.51	−0.02	−0.02
			$(M-N)_2$*	−0.36	0.58	−0.12	0.00	0.63	−0.51	0.02	−0.02
Br	W	1	$(M-N)_1$	0.64	0.40	−0.01	0.07	0.24	0.47	0.00	−0.01
			$(M-N)_2$	−0.64	0.40	0.01	0.07	−0.24	0.47	0.00	−0.01
			$(M-N)_1$*	0.36	0.57	0.15	−0.03	−0.63	−0.50	0.02	0.03
			$(M-N)_2$*	−0.36	0.57	−0.15	−0.03	0.63	−0.50	−0.02	0.03

present paper we provide a more detailed discussion of our previous $[MoCl_4N]_2$ studies as well as new results on periodic trends for $[MX_4N]_2$ complexes. Specifically, we have examined halogen substitution (X = F, Cl, and Br) as well as the substitution of tungsten for molybdenum.

Results and Discussion

Our initial theoretical efforts[17] have been directed at providing energetic support for the kinetic (low activation energy) and thermodynamic accessibility of **1** for $[Cl_4MoN]_2$. We find[17] this valence-bond structure is accessible; however, it is not the most stable "valence isomer". The classical structure **2** is more stable than the activated structure **1** by 21 kcal/mol. The valence orbitals for $[Cl_4MoN]_2$, at the optimized geometries associated with valence-bond structures **1** and **2**, are given in Figures 4 and 5, respectively. As expected, for **1**, there are two metal–ligand covalent π bonds, whereas for **2**, there is a nitrogen–nitrogen π bond and a metal–metal π–π* interaction pair.

The natural orbitals from which the plots in Figures 4 and 5 were derived have been transformed to a fragment basis (as discussed in Appendix II), and the results are tabulated in Table I. We find, for classical structure **2**, the simple correlation diagram shown in Figure 2 adequately describes the metal–nitrogen interactions, in agreement with previous theoretical work.[11-13,15] The lowest π orbital is predominantly N–N bonding (Table I, row 5). The next π orbital (row 6) is mainly M–M π antibonding, due to the orthogonality constraints imposed on the M–M π-bonding orbital by the lower energy N–N π-bonding orbital. The M–M π-bonding orbital is next (row 7), and the N–N π-antibonding orbital is highest (row 8). A single fragment orbital is dominantly used in each of these molecular orbitals. Further, the complementary double-ζ component fragment orbitals are used sparingly, indicating that the fragment-based description is quite reasonable.

For structure **1**, linear combinations of the fragment orbitals are used to form localized M–N π bonds and antibonds (rows 1 through 4 of Table I), in support of the correlation diagram in Figure 3. For the Mo–N π bonds, the M–M π-antibonding fragment orbital is used more than the π-bonding fragment orbital because the two Mo–N π bonds in each plane must remain orthogonal to each other. The analogous situation occurs for the Mo–N π* orbitals as well, except for this case the N–N π-antibonding fragment orbital is used more than the N–N π-bonding fragment orbital (rows 3 and 4 of Table I).

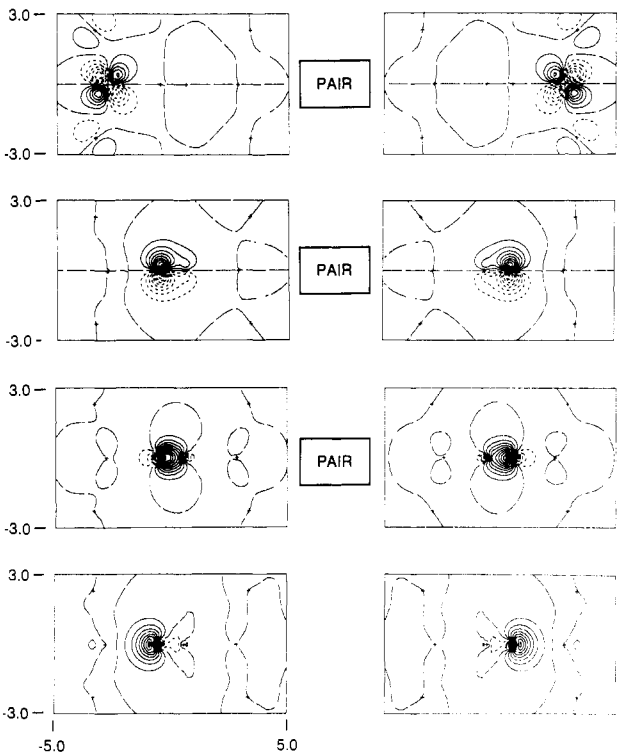

Figure 4. Contour plots of the GVB orbitals defining the molybdenum–nitrogen interactions for the classical form of $[MoCl_4N]_2$. The orbital-plotting plane contains two chlorines, both molybdenums, and both nitrogens. The top two orbitals form one of the two molybdenum interaction pairs. The second pair of orbitals is one of the two N–N π bonds. The third pair is the N–N σ bond. The bottom two orbitals are the nitrogen lone pairs.

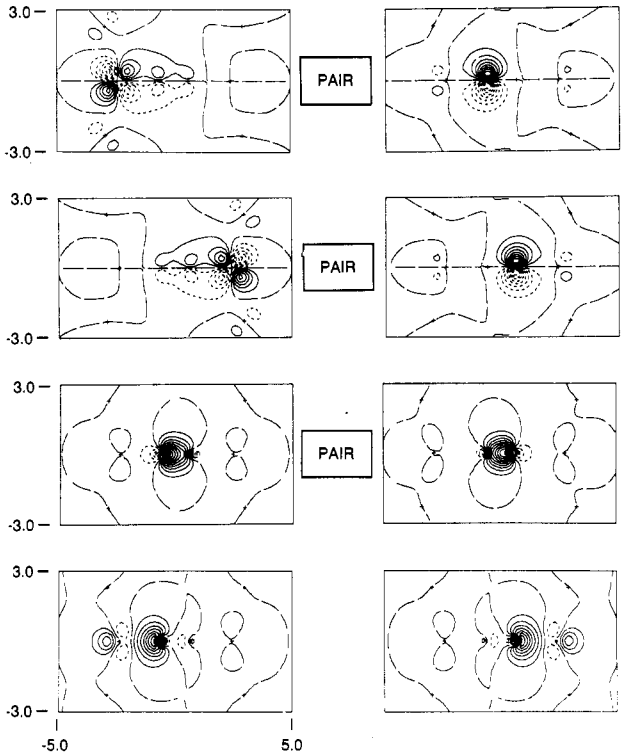

Figure 5. Contour plots of the GVB orbitals defining the molybdenum–nitrogen interactions for the activated (azine) form of $[MoCl_4N]_2$. The orbital-plotting plane contains two chlorines, both molybdenums, and both nitrogens. The top two orbitals form one of the four molybdenum–nitrogen π-bond pairs. The second pair of orbitals forms the second of the two molybdenum–nitrogen π-bond pairs in the plot plane. The third pair is the N–N σ bond. The bottom two orbitals are the nitrogen lone pairs.

Table II. $[X_4MoN-]_2$ Trends

X	Mulliken charge on X	Mo–N π overlap	$E_{N_2} - E_{azine}$, kcal/mol	ionic bond strength, kcal/mol	pop. in d_{xy}
F	−0.57	0.595	41	85–94	0.33
Cl	−0.24	0.618	21	61–67	0.47
Br	−0.18	0.637	15	46–52	0.50

Stabilization of the activated structure **1** should result if the ligand backbone or metal is changed to a combination providing stronger metal–nitrogen covalent π bonds. For example, addition of σ-donor ligands such as phosphines, amines, or ethers will expand the metal d orbitals, enhancing the overlap with the nitrogen p orbitals and thus increasing the metal–nitrogen π-bond strengths. Alternately, substituting tungsten for molybdenum will inherently increase the size of the d orbitals, thus strengthening the metal–nitrogen π bonds. Finally, substitution with less electronegative ligands will also expand the d orbitals, increasing the Mo–N π-bond strengths.

There are limits to the degree of stabilization desired: if **1** were significantly more stable than **2**, then **1** would be thermodynamically inert to low-energy reaction with reductants as mild as H_2. This is because NH_3 is only 4 kcal/mol below $^1/_2\ N_2 + {}^3/_2\ H_2$ and a N_2 complex substantially more stable than free N_2 could not form NH_3 from H_2 due to the endothermicity of the reaction.

Molybdenum. The data presented in Table II computationally confirm our previous suggestion[17] that the relative stability of a normal dinitrogen bridge **2** over the activated form **1** is inversely related to the electronegativity or ionic bond strength of the halogen–ligand set: the energy difference between **2** and **1** decreases in the order F > Cl > Br. The ionic bond strengths reported in Table II are discussed in Appendix I. The theoretical details are discussed in Appendix II. Further, the Mo–N π-bond one-electron orbital overlaps reported in Table II reflect the trends anticipated. That is, as the ionic bond strength of the halogen

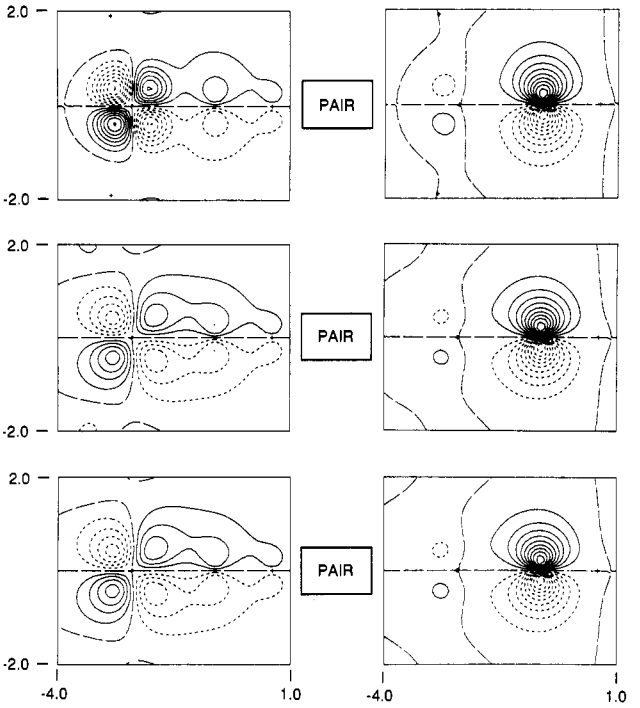

Figure 6. Contour plots of the GVB orbitals defining one of the molybdenum–nitrogen π-bond interactions for the activated (azine) form of $[MoX_4N]_2$. The orbital-plotting plane contains two halogens, both molybdenums, and both nitrogens. The top two orbitals form one of the four molybdenum–nitrogen π-bond pairs for the octafluoro complex. The second pair of orbitals forms one of the four molybdenum–nitrogen π-bond pairs for the octachloro complex. The third pair of orbitals forms one of the four molybdenum–nitrogen π-bond pairs for the octabromo complex.

Table III. Relative Ionic Bond Strengths

X	EA(X), kcal/mol	Mo–X ionic bond strength estimates	
		R, Å	bond strength, kcal/mol
F	78.4	1.85–1.95	94–85 (110)
Cl	83.4	2.25–2.35	67–61
Br	77.6	2.40–2.50	52–46
I	70.6	2.63–2.73	33–28
OH	42.1	1.90–2.00	53–44
SH	53.5	2.30–2.40	34–28
Cp	41.2	2.20–2.30	28–21

Table IV. $[X_4WN-]_2$ Trends

X	Mulliken charge on X	W–N π overlap	$E_{N_2} - E_{azine}$, kcal/mol	ionic bond strength, kcal/mol	pop. in d_{xy}
F	−0.71	0.654	−53	85–94	0.20
Cl	−0.30	0.669	−57	61–67	0.49
Br	−0.35	0.667	−48	46–52	0.50

decreases, there is less charge withdrawn from the metal, and as a result, the metal d orbitals expand, increasing their overlap with the nitrogen p orbitals. Note, also, the net charge (based upon a Mulliken analysis) on the halogen also follows the electronegativity or ionic bond strength expectations. The orbital contour plots in Figure 6 for the Mo–N π bonds of F, Cl, and Br complexes visually amplify the above numerical arguments concerning orbital size and orbital overlap. The data in rows 17–24 of Table I indicate that the bonding interactions for F and Br are essentially the same as for Cl. For molybdenum, halogen substitution is not enough of a perturbation to preferentially activate N_2; the normal dinitrogen form **2** is still favored over the activated (azine) form **1**. As discussed in Appendix I, it is straightforward to determine ionic bond strengths for other two-electron-donor ligands, and comparable ionic bond strengths are provided in Table III for such ligands. The data suggest ligands sufficiently less electronegative

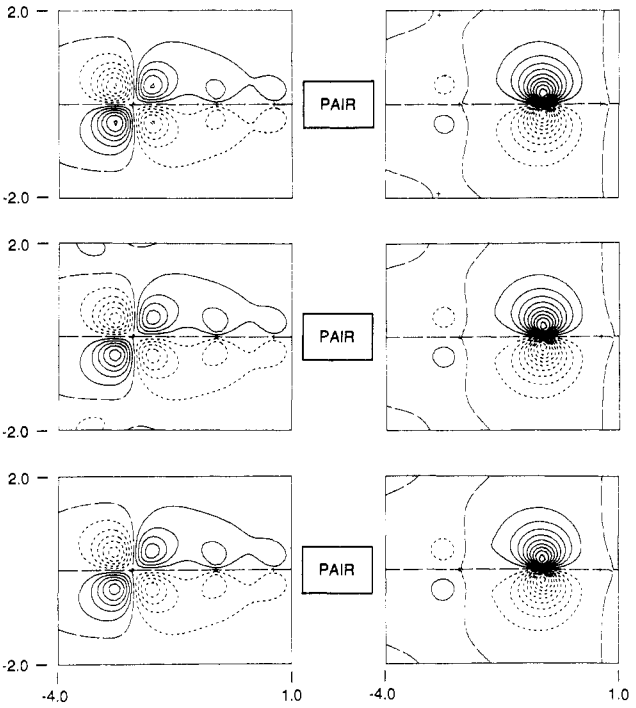

Figure 7. Contour plots of the GVB orbitals defining one of the tungsten–nitrogen π-bond interactions for the activated (azine) form of $[WX_4N]_2$. The orbital-plotting plane contains two halogens, both tungstens, and both nitrogens. The top two orbitals form one of the four tungsten–nitrogen π-bond pairs for the octafluoro complex. The second pair of orbitals forms one of the four tungsten–nitrogen π-bond pairs for the octachloro complex. The third pair of orbitals forms one of the four tungsten–nitrogen π-bond pairs for the octabromo complex.

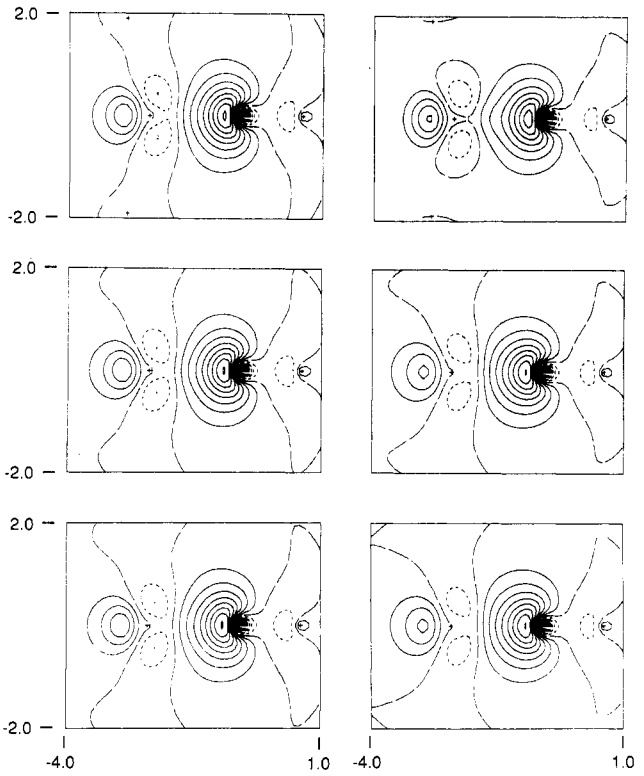

Figure 8. Contour plots of the doubly occupied nitrogen lone-pair orbitals for the fluoro, chloro, and bromo molybdenum and tungsten $[MX_4N]_2$ complexes. The orbital-plotting plane contains two halogens, both metals, and both nitrogens. The top left orbital is from the molybdenum octafluoro complex. The top right orbital is from the tungsten octachloro complex. The middle left orbital is from the molybdenum octachloro complex. The middle right orbital is from the tungsten octabromo complex. The bottom left orbital is from the molybdenum octabromo complex. The bottom right orbital is from the tungsten octabromo complex.

than bromide, e.g. alkoxide or thiolate, may preferentially stabilize form **1** over form **2**.

Tungsten. As seen from the data presented in Table IV, replacing Mo with W preferentially stabilizes the activated form **1**, but the stabilization is too large (below the threshold for forming NH_3). Note also from Table IV that for tungsten, in contrast to molybdenum, halogen substitution has very little effect on M–N π-bond overlap and consequently **1** vs. **2** stability. The W–N π-bond overlap is nearly independent of the halogen used (Table IV), and further ligand substitution should not bring structures **1** and **2** closer together energetically (plots of the orbitals are shown in Figure 7). These energetic differences do not manifest themselves in radically different electronic structures for the tungsten complexes relative to the molybdenum complexes. The similarity of the electronic structures may be seen by comparing analogous rows of Table I (for example rows 17 and 25 should be compared) and comparing appropriate plots from Figures 6 and 7.

The optimized geometries for the octachloro azine complexes of Mo and W differ in a manner consistent with the energetic results discussed above. The N–N bond for the Mo complex is shorter and hence less activated than that for the W complex (1.23 Å for Mo compared to 1.27 Å for W). Further, the M–N bond distance is substantially shorter for the W complex (1.75 Å) than for the Mo complex (1.80 Å). For comparison, the X-ray structure for $[W(PhC{\equiv}CPh)CH_3OCH_2CH_2OCH_3)Cl_2N]_2$ yielded W–N distances of 1.776 and 1.735 Å (average of 1.756 Å). For this complex a N–N distance of 1.292 Å was determined.

Conclusions

Ligand substitution and metal replacement does affect the relative stability of the two bridging dinitrogen isomers **1** and **2**. Modification of molybdenum complexes (as described above) is probably the more viable approach to obtaining an active dinitrogen activation catalyst; tungsten complexes have been found to be just too stable. Each of the three tungsten complexes studied is substantially below the threshold for forming NH_3.

Table V. Total Energies (hartrees)

X	M	1	2
F	Mo	−431.810 759	−431.888 360
Cl	Mo	−359.274 037	−359.304 119
Br	Mo	−344.699 954	−344.724 706
F	W	−434.028 464	−433.944 615
Cl	W	−361.270 318	−361.179 822
Br	W	−349.510 560	−346.433 936

Acknowledgment. The author thanks Dr. Carla Casewit for helpful discussions. This work is supported by NSF Grant CHE-8405399. Acknowledgment is made to the CSU Supercomputing Project for partial support of this research.

Appendix I

A qualitative (semiquantitative) energetic description of ionic bonding,[20] if it is idealized as A^+B^-, is

$$E_{ionic} = IP_A - EA_B - 1/R_{AB} + PR \qquad (A1)$$

where IP_A is the ionization potential of the species likely to lose the electron (A), EA_B is the electron affinity of the species that is likely to receive the electron (B), $1/R_{AB}$ is the electrostatic attraction between the two species, A and B, and PR signifies the Pauli repulsion interactions between the two species. Equation A1, while only being qualitative, does provide a reasonable estimate of relative ionic bond strengths for comparable B ligands, given a common metal A.[21] If ligand B_1 bonded to A has a smaller ionic bond strength than ligand B_2 bonded to A, then there is a

(20) Pauling, L. *J. Am. Chem. Soc.* **1932**, *54*, 3570–3582.
(21) Allison, J. N.; Cave, R. J.; Goddard, W. A., III *J. Phys. Chem.* **1984**, *88*, 1262–1268.

likelihood of more covalency in the bonding of B_1 to A than for ligand B_2 bonded to A. This also implies there will be a tendency for less electron density to be transferred from A to B_1 than from A to B_2. On the basis of reasonable estimates for R_{AB}, ionic bond strengths for several 2e donors are provided in Table III. These energies have been used to develop a scale of electron-withdrawing ability for 2e donors:

$$F > Cl > OH \approx Br > SH \approx I > Cp \qquad (A2)$$

This ordering agrees with that found for the metal Mulliken populations (charges) for MoX_4 complexes (Table II). The data in Table III can also be used to extrapolate the energy differences in Table II to other 2e donors.

Appendix II

The energetics discussed in the text and presented in Tables II and IV are differences between CI[22] calculations at the geometries optimized[17] for $MoCl_4$ complexes **1** and **2**. For all calculations the M–F, –Cl, and –Br distances were fixed at 1.95, 2.35, and 2.50 Å, respectively. The N–M–X bond angle was fixed at 103°, and a D_{4h} geometry was retained throughout.

For both valence-bond structures for N–N σ-bond pair and the nitrogen s lone pairs were explicitly correlated. In addition, for structure **1** the four M–N π bonds were correlated. For structure **2** the two N–N π bonds were correlated as well as the two Mo–Mo spin-paired π interactions. For each case a CI calculation was performed consisting of a full CI within each of the two four-orbital π spaces and single excitations within the six σ orbitals. An overall limitation of quadrupole excitations was applied. The final configuration list consisted of 4768 spin eigenfunctions and 18 455 determinants.

Effective potentials were utilized on all centers except nitrogen. The chlorine potential is from Rappé, Smedley, and Goddard.[23] The remaining potentials are from Hay and Wadt.[24] A benchmark calculation on Cl_4MoO yielded a GVB–CI Mo–O bond distance of 1.713 Å compared to 1.702 Å for the analogous calculation where the Mo center was treated all electron. The effective potential on Mo replaced the electrons up through $n = 3$. The effective potential on W replaced the electrons up through $n = 4$. The remaining electrons were represented with valence double-ζ basis sets.[23-25] Total energies for each structure are given in Table V. For **1**, M = W and X = Cl, we optimized the W–N and N–N distances. For Cl_4WO we calculate a W–O distance of 1.70 Å; experimentally this distance is 1.73 Å. For Cl_4WO we calculate a W–O distance of 1.70 Å; experimentally this distance is 1.73 Å. An average experimental W–N(azine) bond distance is 1.756 Å; we calculate this distance to be 1.80 Å.

The transformation from molecular orbitals in an atomic basis to molecular orbitals in a fragment basis was accomplished with

$$\mathbf{T} = \mathbf{B}^{-1}\mathbf{T}^{T}_{frag}\mathbf{T}_{ao} \qquad (A3)$$

where $\mathbf{T}_{frag}$ is the molecular orbital coefficient matrix over atomic orbitals for the molecular fragments. $\mathbf{T}_{ao}$ is the molecular orbital coefficient matrix over atomic orbitals for the actual molecule (generated using a GVB–PP wavefunction). **T** is the molecular orbital coefficient matrix over a fragment orbital basis for the actual molecule. $\mathbf{B}^{-1}$ is the inverse of **B**

$$\mathbf{B} = \mathbf{T}^{T}_{frag}\mathbf{T}_{frag} \qquad (A4)$$

which is the symmetrized form of the fragment orbital matrix over atomic orbitals.

Note Added in Proof. Bercaw and co-workers have reported the addition of dihydrogen across the metal–nitrogen π bond in the complex $Cp_2^*ScNHPh$.[26]

Registry No. $[Cl_4MoN-]_2$, 69492-89-3; $[Cl_4WN-]_2$, 105102-34-9; $[F_4MoN-]_2$, 105102-35-0; $[Br_4MoN-]_2$, 105102-36-1; $[F_4WN-]_2$, 105102-37-2; $[Br_4WN-]_2$, 105102-38-3.

(22) Shavitt, I. In *Modern Theoretical Chemistry: Methods of Electronic Structure Theory*; Schaefer, H. F., III, Ed.; Plenum: New York, 1977; Vol. 3, Chapter 6, pp 189–275.
(23) Rappé, A. K.; Smedley, T. A.; Goddard, W. A., III. *J. Phys. Chem.* **1981**, *85*, 1662–1666.
(24) Hay, P. J.; Wadt, W. R. *J. Chem. Phys.* **1985**, *82*, 270–283. Wadt, W. R.; Hay, P. J. *J. Chem. Phys.* **1985**, *82*, 284–298.
(25) Rappé, A. K.; Goddard, W. A., III, unpublished results.
(26) Bercaw, J. E.; Davies, D. L.; Wolczanski, P. T. *Organometallics* **1986**, *5*, 443–450.